RFI and Mainlobe Jamming Mitigation for Multi-channel Imaging Radars

Patrick Bidigare

Veridian Systems
3300 Plymouth Rd.
Ann Arbor, MI 48130
bidigare@erim-int.com

ABSTRACT

A common approach to suppressing jamming or RFI is (adaptive) beamforming, where an antenna pattern null is formed by appropriately combining multiple receive channels. A sidelobe canceller is a common such implementation.

Beamforming is undesireable when the interference source is in the mainlobe of the radar, because the antenna pattern null created by the beamformer produces a region where ground imaging cannot be performed.

This paper presents two conceptual alternatives to spatial beamforming. The first approach produces a SAR image by combining the pulse returns from multiple channels in a non-separable way. This "space time beamforming" is shown to produce a null which is significantly narrower and shallower than that produced by conventional spatial beamforming. Further, we demonstrate that the space time beamforming null becomes narrower as the length of the synthetic aperture (i.e. the doppler resolution) increases.

A second alternative to spatial beamforming is presented which is useful when the interference source is non-white or when it is desirable to estimate the (spatially localized) interfering signal. This signal separation approach allows generic localized sources such as moving target signatures, vibrating target paired echoes, etc. to be separated from the clutter data.

1. INTRODUCTION

A typical approach to radio frequency interference (RFI) and jamming suppression for multi-channel radars is (spatial) beamforming [1]. Here, a linear combination of receive channels is used to produce an antenna pattern null on receive in the direction(s) of the interference. A sidelobe canceller is a common such implementation.

Spatial beamforming works well when the RFI source is in the sidelobes of the radar, however in the mainbeam, spatial beamforming produces a deep, wide notch. For imaging radars, this notch produces a region where clutter reflectivity cannot be estimated.

In this paper we present two alternative approaches to spatial beamforming. The first uses non-separable space time beamforming to produce a much narrower, shallower null. The second approach provides a method for separating the clutter and localized interference signals when both of these are of interest. We compare the performance of spatial beamforming vs. space time beamforming in terms of the width and depth of the clutter notch produced.

Consider SAR image formation as a problem of estimating the radar cross section of each range/Doppler cell in the presence of thermal noise and localized RFI. We consider the width of the region of range/Doppler cells whose Cramer-Rao variance bounds exceed a given threshold. We show that the non-separable spatial (multiple channels) and temporal (multiple pulses) processing, produces a much narrower null width (as defined above) than conventional separable beamforming.

The example results shown in this utilize video phase history data collected by Veridian System's DCS radar with synthetic RFI introduced prior to image formation.

The author would like to thank Mike Beauvais for his help with producing the examples shown in the paper and Mark Stuff for several interesting discussions.

2. TECHNICAL DISCUSSION

2.1 Spatial Beamforming

A typical approach to RFI suppression is adaptive beamforming. Here, a particular coherent combination of the receive channels from a multi-channel antenna is chosen so as to maximize the signal to interference plus noise (SINR) ratio in a particular steering direction. This is illustrated in Figure 1 and Figure 2.

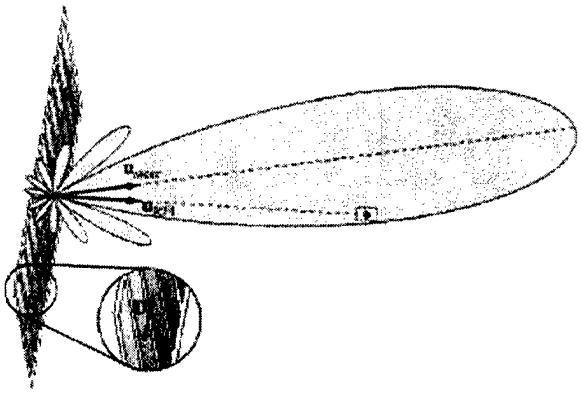

Figure 1: Multi-channel antenna

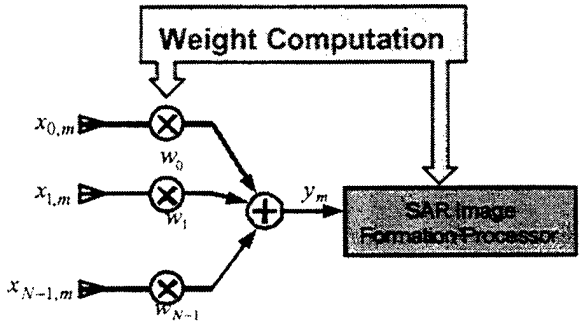

Figure 2: Beamforming applied to SAR imaging.

The Gauss-Markov theorem provides a closed-form for the weight vector $\mathbf{w}$ which maximizes this SINR when the covariance of the interference and noise are known.

We model our interference covariance as the sum of a spatially white thermal noise term with variance σ_n^2 and a (rank 1) spatially localized RFI term which is the outer product of the steering vector $\mathbf{z}_{\mathbf{RFI}} = (z_{RFI}^0, \ldots, z_{RFI}^{N-1})$ to the RFI source with itself.

$$\underset{\text{interference}}{\mathbf{R_u}} = \underset{\text{noise}}{\mathbf{R_n}} + \underset{\text{RFI}}{\mathbf{R_j}} = \sigma_n^2 \begin{bmatrix} 1 & 0 & \cdots & 0 \\ 0 & 1 & & 0 \\ \vdots & & \ddots & \\ & & & \end{bmatrix} + \sigma_j^2 \begin{bmatrix} z_{RFI}^0 & z_{RFI}^1 & \cdots & z_{RFI}^{N-1} \\ z_{RFI}^{-1} & z_{RFI}^0 & & z_{RFI}^{N-2} \\ \vdots & & \ddots & \\ z_{RFI}^{1-N} & z_{RFI}^{2-N} & & z_{RFI}^0 \end{bmatrix}$$

Here $z_{\mathrm{RFI}} = \exp\left\{2\pi\, i \dfrac{\mathbf{D}\cdot\mathbf{u}_{\mathrm{RFI}}}{\lambda}\right\}$ is the complex root of unity corresponding to the channel-to-channel phase change due to the position of the RFI source in the scene (see Figure 1).

The weight vector is given by

$$\mathbf{w} = \mathbf{R}_{\mathbf{u}}^{-1}(\,\mathbf{z}_{\mathbf{steer}} \cdot \mathbf{t}\,),$$

where $\mathbf{t}$ is a tapering vector and . denotes the Hadamard (pointwise) product. The weight vector is optimal when $\mathbf{t} = (1,1,\ldots,1)$, however for purposes of sidelobe reduction, a weighted taper is generally used.

A typical implementation of beamforming is a sidelobe canceller. Here the main subarrays of the antenna are used for beamsteering and a small number of auxiliary channels are then adaptive combined with the main channel for RFI cancellation in the sidelobes.

Beamforming can be applied to SAR image formation by first forming a coherent (spatial) combination of the receive channels and then passing this into a SAR image formation processor which then forms the temporal combination of received pulses appropriate to scene reconstruction. This approach is shown in Figure 2.

This separable spatial-then-temporal processing works well when the RFI source occurs in the sidelobes, but has undesirable effects as the RFI source enters the mainlobe. The –40dB Taylor tapered adapted antenna patterns for various RFI source locations are shown in Figure 3.

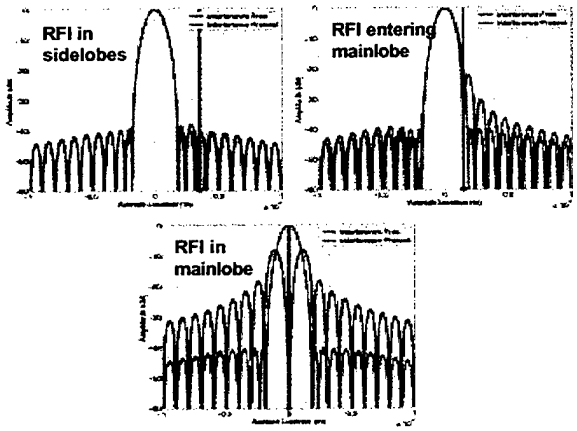

Figure 3: Beamformer antenna patterns.

As can be seen, an RFI source in the sidelobes has very little effect on the sidelobe levels or on the mainlobe shape. However as soon as the source enters the mainlobe, the sidelobe levels rise and the mainlobe distorts. The worst degradation occurs when the RFI source coincides with the beamsteering direction. In this case a wide, deep notch appears in the mainbeam and the sidelobes are elevated by 20dB.

2.2 Space Time Beamforming

The problem inherent with separable spatial-then-temporal beamforming for SAR imaging is that the optimal weights maximize the SINR only in the steering direction. Simultaneous maximization of SINR in all directions inherently requires a non-separable approach. To develop

such an approach, we consider the very simple DPCA data model shown in Figure 4.

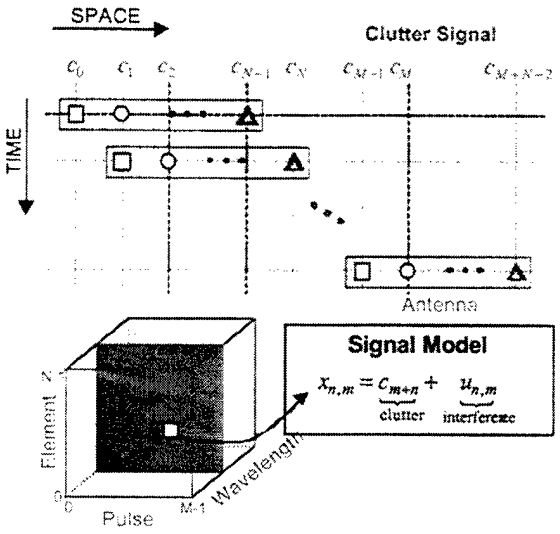

Figure 4: Space time signal model.

Here a received data sample shown in the radar data cube is indexed by channel (element), pulse and wavelength and consists of a deterministic clutter coefficient and a random noise + RFI component. We model the clutter as stationary and thus dependent only on the spatial location of the receiving antenna phase center. For illustration, we consider the simple DPCA situation where the antenna moves one phase center spacing between pulses. In this case, the clutter coefficient c_{m+n} in $x_{n,m}$ depends on the sum $m+n$.

Written as a matrix equation in the case of $M=4$ pulses and $N=3$ channels we have

$$\underbrace{\begin{bmatrix} x_{0,0} \\ x_{0,1} \\ x_{0,2} \\ x_{0,3} \\ \hline x_{1,0} \\ x_{1,1} \\ x_{1,2} \\ x_{1,3} \\ \hline x_{2,0} \\ x_{2,1} \\ x_{2,2} \\ x_{2,3} \end{bmatrix}}_{\mathbf{x}} = \underbrace{\left[\begin{array}{cccccc} 1 & 0 & 0 & 0 & 0 & 0 \\ 0 & 1 & 0 & 0 & 0 & 0 \\ 0 & 0 & 1 & 0 & 0 & 0 \\ 0 & 0 & 0 & 1 & 0 & 0 \\ \hline 0 & 1 & 0 & 0 & 0 & 0 \\ 0 & 0 & 1 & 0 & 0 & 0 \\ 0 & 0 & 0 & 1 & 0 & 0 \\ 0 & 0 & 0 & 0 & 1 & 0 \\ \hline 0 & 0 & 1 & 0 & 0 & 0 \\ 0 & 0 & 0 & 1 & 0 & 0 \\ 0 & 0 & 0 & 0 & 1 & 0 \\ 0 & 0 & 0 & 0 & 0 & 1 \end{array}\right]}_{\mathbf{Z}} \underbrace{\begin{bmatrix} c_0 \\ c_1 \\ c_2 \\ c_3 \\ c_4 \\ c_5 \end{bmatrix}}_{\mathbf{c}} + \underbrace{\begin{bmatrix} u_{0,0} \\ u_{0,1} \\ u_{0,2} \\ u_{0,3} \\ \hline u_{1,0} \\ u_{1,1} \\ u_{1,2} \\ u_{1,3} \\ \hline u_{2,0} \\ u_{2,1} \\ u_{2,2} \\ u_{2,3} \end{bmatrix}}_{\mathbf{u}},$$

We model the interference as consisting of a spatially and temporally white noise component and a spatially localized and temporally white RFI source.

$$\mathbf{R_u} = \underbrace{\left(\sigma_n^2 \begin{bmatrix} 1 & 0 & 0 \\ 0 & 1 & 0 \\ 0 & 0 & 1 \end{bmatrix} + \sigma_j^2 \begin{bmatrix} z_j^0 & z_j^1 & z_j^2 \\ z_j^{-1} & z_j^0 & z_j^1 \\ z_j^{-2} & z_j^{-1} & z_j^0 \end{bmatrix} \right)}_{\text{spatialcovariance}} \otimes \underbrace{\begin{bmatrix} 1 & 0 & 0 & 0 \\ 0 & 1 & 0 & 0 \\ 0 & 0 & 1 & 0 \\ 0 & 0 & 0 & 1 \end{bmatrix}}_{\text{temporalcovariance}}$$

Here $z_j = \exp\left\{2\pi i \frac{\mathbf{D}\cdot\hat{\mathbf{u}}_j}{\lambda}\right\}$ is complex root of unity corresponding to the position of the RFI source as shown in Figure 5.

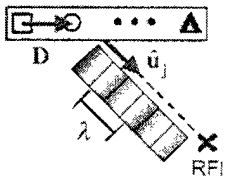

Figure 5: RFI source geometry.

The Gauss-Markov theorem can be used to construct the best linear unbiased estimator for the clutter coefficients in this colored interference environment. The clutter estimator is given by

$$\mathbf{c} = (\mathbf{Z}^H \mathbf{R}_u^{-1} \mathbf{Z})^{-1} \mathbf{Z}^H \mathbf{R}_u^{-1} \mathbf{x}$$

The purpose of this paper is to present and compare conceptual approaches to RFI suppression without introducing actual algorithms, however it's worth noting that the BLUE for clutter coefficient estimation has a matrix structure (Figure 6) which makes it particularly amenable to solution using linear solvers. Evaluation of the matrix-vector product $\mathbf{Z}^H \mathbf{R}_u^{-1} \mathbf{x}$ amounts to evaluating the Z-transform of $\mathbf{x}$ at various locations and thus can be efficiently evaluated using the chirp-Z transform. Further, it's straightforward to show that the matrix $\mathbf{Z}^H \mathbf{R}_u^{-1} \mathbf{Z}$ has a banded matrix structure with upper and lower bandwidths $N-1$, thus efficient sparse matrix solvers can be applied.

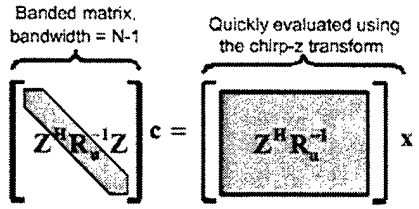

Figure 6: Space time beamforming matrix structure.

Figure 7 shows the results of the separable spatial beamforming and non-separable space-time beamforming approaches applied to real SAR video phase history with synthetic RFI.

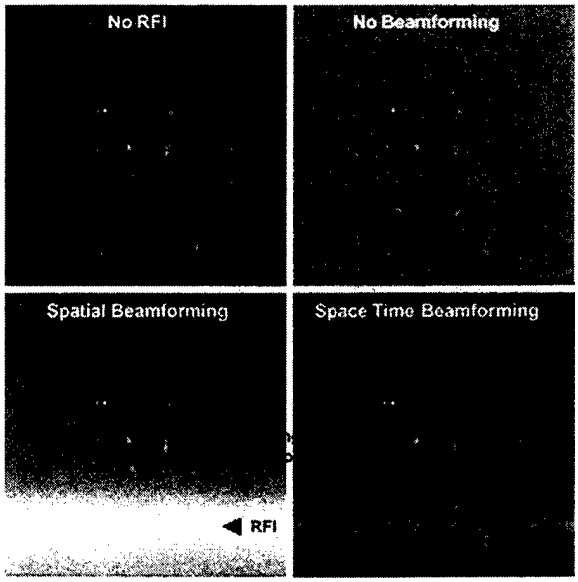

Figure 7: Spatial vs. space time beamforming.

This example corresponds to a radar with a standoff range of 100km, having a 3m antenna. The simulation uses a CNR of 26dB and a JNR of 38dB with $N = 6$ channels and $M = 2750$ pulses.

The separable spatial beamforming null is seen to be deeper and wider than its space-time counterpart. In fact, the SINR in the direction of the RFI is actually worse than had no beamforming been performed. This is because the separable beamforming is only optimal in the steering direction. The space time beamformer is never any worse than the case of no beamforming and recovers most of the image everywhere but very near the RFI source.

2.3 Beamforming Comparison

The spatial and space time beamforming approaches to RFI suppression can be compared somewhat more rigorously by considering the clutter to noise ratios produced by these methods as a function of the azimuth position of a clutter patch and the azimuth position of the RFI source. These clutter to noise ratios are given by

$$CNR_{\text{spatial}} = M \frac{\left((\mathbf{v}_{\text{steer}} \cdot \mathbf{t})^H \mathbf{R}_{\mathbf{u}}^{-1} \mathbf{v}_{\text{clut}}\right)^2}{(\mathbf{v}_{\text{steer}} \cdot \mathbf{t})^H \mathbf{R}_{\mathbf{u}}^{-1} (\mathbf{v}_{\text{steer}} \cdot \mathbf{t})}$$

and

$$CNR_{\text{space-time}} = \frac{(t_0 + t_1 + \cdots + t_{M+N-2})^2}{(\mathbf{v}_{\text{clut}} \cdot \mathbf{t})^H \left(\mathbf{Z}^{\mathbf{H}} \mathbf{R}_{\mathbf{u}}^{-1} \mathbf{Z}\right)^{-1} (\mathbf{v}_{\text{clut}} \cdot \mathbf{t})}$$

These clutter to noise ratios for the spatial and space time beamforming are shown in Figure **8**.

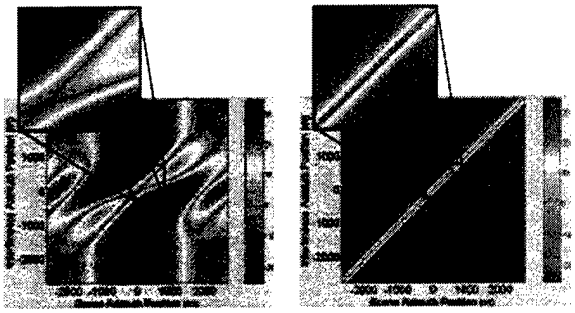

Figure 8: CNR for spatial (left) vs. space time (right) beamforming.

The x-axis corresponds to the azimuth position of the clutter patch and the y axis is the azimuth position of the RFI over a 5km scene. The effects of the RFI position (mainlobe vs. sidelobe) on the spatial beamforming are evident here. No antenna pattern can be seen for the space time beamforming because the individual subarrays patterns were not modeled.

The width of the "notch" produced by beamforming can be defined in terms of a minimally acceptable CNR level. Figure **9** compares the two approaches as the number of pulses used increases (and the doppler resolution gets finer). As can be seen, the spatial beamformer produces a null whose depth is relatively independent of the number of pulses used and whose width improves only slowly with increasing doppler resolution. By contrast, the depth of the space time beamformer notch rises as the number of pulses increases and the width improves dramatically with increasing doppler resolution.

This observation suggests that the width of the null is proportional to the doppler resolution for space time beamforming, although the author has not proven or disproved this as yet.

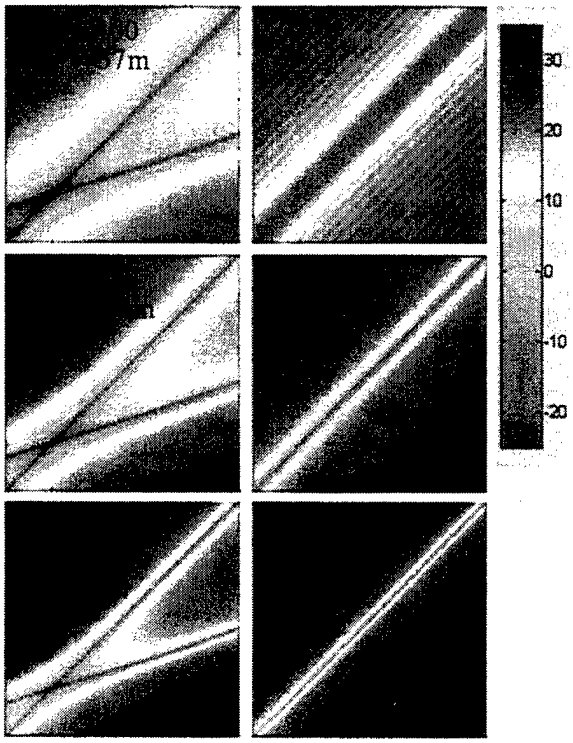

Figure 9: CNR comparison of spatial (left) vs. space time (right) beamforming at various doppler resolutions.

2.4 Signal Separation

Space time beamforming is a potentially useful technique for suppressing RFI in the mainlobe, however in some situations, the interference may be temporally colored or even highly structured. Further, for many applications, the "RFI" may correspond to a spatially localized signal of interest. Such signals can include covert RF tag communication signals, paired echoes from rotating or vibrating objects [3] or even returns from moving targets [2,4,5] where an objective might be to image the moving targets.

In such situations, we would like a method for extracting the clutter signal from the localized source. Figure **10** illustrates the distribution of clutter and localized source energy in the radar data cube. The relation between the azimuth location of a stationary patch of clutter and the doppler frequency it manifests causes the clutter energy to concentrate onto a 2D "clutter ridge". The localized source energy also concentrates onto a plane at the azimuth location of the source. It's reasonable to expect, then, that these signals can be separated except where they intersect in the data cube.

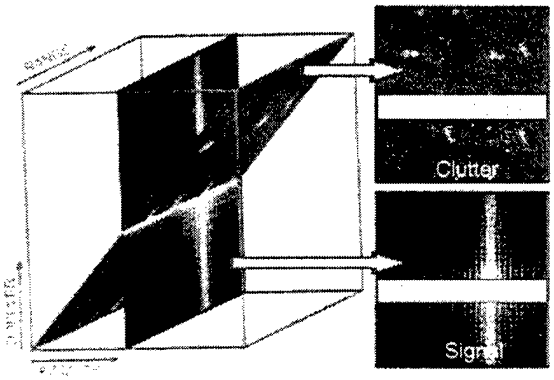

Figure 10: Signal separation cartoon.

We introduce another data model in which both the clutter and the localized source are deterministic quantities. The interference in this case is simply white thermal noise. As before, we model the clutter signal as depending only on the spatial location of the receiving phase center (Figure **11**).

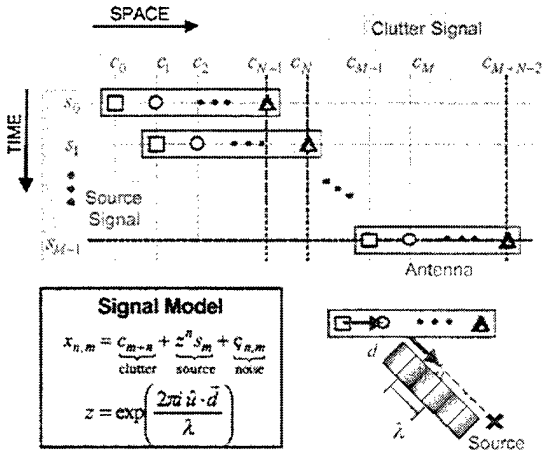

Figure 11: Signal separation data model.

The localized source, on the other hand, is modeled as the product of a temporal term s_m depending only on the pulse number, and spatial term z^n depending on the phase center n and azimuth position z of the source. In matrix notation, we have

$$\underbrace{\begin{bmatrix} x_{0,0} \\ x_{0,1} \\ x_{0,2} \\ x_{0,3} \\ \hline x_{1,0} \\ x_{1,1} \\ x_{1,2} \\ x_{1,3} \\ \hline x_{2,0} \\ x_{2,1} \\ x_{2,2} \\ x_{2,3} \end{bmatrix}}_{\mathbf{X}} = \underbrace{\left[\begin{array}{cccccc|cccc} 1 & 0 & 0 & 0 & 0 & 0 & z^0 & 0 & 0 & 0 \\ 0 & 1 & 0 & 0 & 0 & 0 & 0 & z^1 & 0 & 0 \\ 0 & 0 & 1 & 0 & 0 & 0 & 0 & 0 & z^2 & 0 \\ 0 & 0 & 0 & 1 & 0 & 0 & 0 & 0 & 0 & z^3 \\ \hline 0 & 1 & 0 & 0 & 0 & 0 & z^0 & 0 & 0 & 0 \\ 0 & 0 & 1 & 0 & 0 & 0 & 0 & z^1 & 0 & 0 \\ 0 & 0 & 0 & 1 & 0 & 0 & 0 & 0 & z^2 & 0 \\ 0 & 0 & 0 & 0 & 1 & 0 & 0 & 0 & 0 & z^3 \\ \hline 0 & 0 & 1 & 0 & 0 & 0 & z^0 & 0 & 0 & 0 \\ 0 & 0 & 0 & 1 & 0 & 0 & 0 & z^1 & 0 & 0 \\ 0 & 0 & 0 & 0 & 1 & 0 & 0 & 0 & z^2 & 0 \\ 0 & 0 & 0 & 0 & 0 & 1 & 0 & 0 & 0 & z^3 \end{array}\right]}_{\mathbf{Z}} \underbrace{\begin{bmatrix} c_0 \\ c_1 \\ c_2 \\ c_3 \\ c_4 \\ c_5 \\ s_0 \\ s_1 \\ s_2 \\ s_3 \end{bmatrix}}_{\mathbf{CS}} + \underbrace{\begin{bmatrix} u_{0,0} \\ u_{0,1} \\ u_{0,2} \\ u_{0,3} \\ \hline u_{1,0} \\ u_{1,1} \\ u_{1,2} \\ u_{1,3} \\ \hline u_{2,0} \\ u_{2,1} \\ u_{2,2} \\ u_{2,3} \end{bmatrix}}_{\mathbf{u}}$$

Since our interference is spatially and temporally white, the best estimator of the clutter and signal coefficients is the least squares solution

$$\mathbf{CS} = (\mathbf{Z}^{\mathbf{H}}\mathbf{Z})^{-1}\mathbf{Z}^{\mathbf{H}}\mathbf{X}$$

As might be expected, the matrix $\mathbf{Z}$ is not full rank. This rank deficiency corresponds to the intersection region (Figure **10**) between the clutter ridge and localized source. This problem can be corrected by introducing an extra row in $\mathbf{Z}$ which effectively allows us to specify whether the inseparable energy in the intersection should be included with the clutter signal or the localized source signal.

Figure **12** shows the result of applying this signal separation technique to 3 channel SAR video phase history with synthetic RFI and then processing the separated signals into SAR images using a conventional image formation processor.

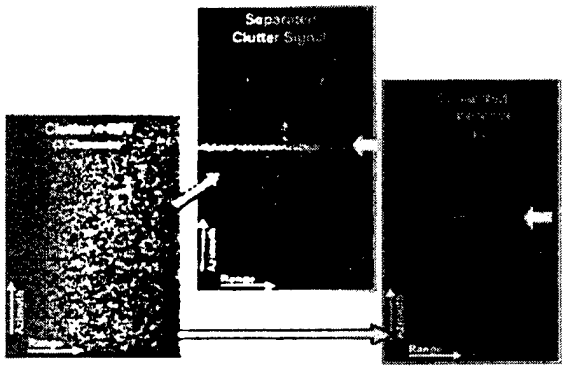

Figure 12: Signal separation example.

Here we used 1024 pulses and set up the simulation to have a CNR of 30dB and a JNR of 40dB. We included the overlap region with the clutter signal.

Our initial results suggest that the width of the intersection region wherein the clutter cannot be discerned from the source is proportional to the doppler resolution of the radar, and thus can be made more narrow by collecting more pulses.

3. CONCLUSIONS + FURTHER WORK

The purpose of this paper was to suggest three conceptual approaches to the problem of RFI mitigation and more generally the problem of separating the clutter signal from a localized source. It was shown that non-separable space time beamforming is necessary to effectively combat mainbeam RFI.

Any practical implementation of these techniques would have to solve three problems not addressed by the paper. The first problem is determining the azimuth position of the RFI or localized source. The second is the estimation of the interference environment (or at very least, the noise σ_n^2 and RFI σ_j^2 variances). Lastly, the problem of channel balancing must be addressed. Innovative adaptive signal processing approaches will be required to solve these problems.

4. REFERENCES

[1] J.R. Guerci, J.S. Goldstein, I.S. Reed, "Optimal and Adaptive Reduced-Rank STAP," *IEEE Transactions on Areospace and Electronic Systems*, vol. 36, no. 2, 2000, pp. 647-663.

[2] J.H.G. Ender, "Space-time processing for multichannel synthetic aperature radar," *Electronics and Communication Engineering Journal*, vol. 1, no. 1, 1999, pp. 29-38.

[3] N.S. Subotic, B.J.Thelen, D.A.Carrara, "Cyclostationary signal models for the detection and characterization of vibrating objects in SAR data," *Proceedings of the 1998 32nd Asilomar Conference on Signals, Systems and Computers*, Part 2 (of 2) Pacific Grove, CA, USA 19981101-19981104 IEEE

[4] S.A. Werness, M.A. Stuff, J.R. Fienup, "Two-dimensional imaging of moving targets in SAR data," *1990 (24th) Asilomar Conference on Signals, Systems and Computers*, Part 1 (of 2).

[5] M.A. Stuff, "Three-dimensional analysis of moving target radar signals: Methods and implications for ATR and feature aided tracking", *Proceedings of the SPIE*, v 3721 1999, pp. 485-496